Full Length Article

Validation and integration tests of the JUNO 20-inch PMT readout electronics

Vanessa Cerrone [a], Katharina von Sturm [a,b,*], Marco Bellato [b], Antonio Bergnoli [b],
Matteo Bolognesi [a,b], Riccardo Brugnera [a,b], Chao Chen [c], Barbara Clerbaux [d], Alberto Coppi [a],
Flavio dal Corso [b], Daniele Corti [b], Jianmeng Dong [e], Wei Dou [e], Lei Fan [c], Alberto Garfagnini [a,b],
Guanghua Gong [e], Marco Grassi [a,b], Shuang Hang [d,j], Rosa Maria Guizzetti [a], Cong He [c], Jun Hu [c],
Roberto Isocrate [b], Beatrice Jelmini [a,b], Xiaolu Ji [c], Xiaoshan Jiang [c,i], Fei Li [c], Zehong Liang [c],
Ivano Lippi [b], Hongbang Liu [f], Hongbin Liu [c], Shenghui Liu [c], Xuewei Liu [e], Daibin Luo [c],
Ronghua Luo [f], Filippo Marini [a,b], Daniele Mazzaro [b], Luciano Modenese [b], Zhe Ning [c], Yu Peng [c],
Pierre-Alexandre Petitjean [d], Alberto Pitacco [b], Mengyao Qi [c], Loris Ramina [b], Mirco Rampazzo [b],
Massimo Rebeschini [b], Mariia Redchuk [b], Andrea Serafini [a,b], Yunhua Sun [c], Andrea Triossi [a,b],
Riccardo Triozzi [a], Fabio Veronese [b], Peiliang Wang [c], Peng Wang [d,j], Yangfu Wang [c],
Yusheng Wang [c], Yuyi Wang [e], Zheng Wang [c], Ping Wei [f], Jun Weng [e], Shishen Xian [g,h],
Xiaochuan Xie [c], Benda Xu [e], Chuang Xu [e], Donglian Xu [g,h], Hai Xu [f], Xiongbo Yan [c,i], Ziyue Yan [c],
Fengfan Yang [c], Yan Yang [f], Yifan Yang [d], Mei Ye [c], Tingxuan Zeng [c], Shuihan Zhang [c],
Wei Zhang [c], Aiqiang Zhang [e], Bin Zhang [e], Siyao Zhao [f], Changge Zi [c], Sebastiano Aiello [k],
Giuseppe Andronico [k], Vito Antonelli [o], Andrea Barresi [p], Davide Basilico [o], Marco Beretta [o],
Augusto Brigatti [o], Riccardo Bruno [k], Antonio Budano [q], Barbara Caccianiga [o], Antonio Cammi [r],
Stefano Campese [a,b], Davide Chiesa [p], Catia Clementi [s], Marco Cordelli [t], Stefano Dusini [b],
Andrea Fabbri [q], Giulietto Felici [t], Federico Ferraro [o], Marco G. Giammarchi [o], Cecilia Landini [o],
Paolo Lombardi [o], Claudio Lombardo [l,k], Andrea Maino [m,n], Fabio Mantovani [m,n],
Stefano Maria Mari [q], Agnese Martini [t], Emanuela Meroni [o], Lino Miramonti [o],
Michele Montuschi [m,n], Massimiliano Nastasi [p], Domizia Orestano [q], Fausto Ortica [s],
Alessandro Paoloni [t], Sergio Parmeggiano [o], Fabrizio Petrucci [q], Ezio Previtali [p],
Gioacchino Ranucci [o], Alessandra Carlotta Re [o], Barbara Ricci [m,n], Aldo Romani [s], Paolo Saggese [o],
Simone Sanfilippo [q,1], Chiara Sirignano [a,b], Monica Sisti [p], Luca Stanco [b], Virginia Strati [m,n],
Francesco Tortorici [l,k], Cristina Tuvé [l,k], Carlo Venettacci [q], Giuseppe Verde [k], Lucia Votano [t]

[a] *Università di Padova, Dipartimento di Fisica e Astronomia, Padova, Italy*
[b] *INFN Sezione di Padova, Padova, Italy*
[c] *Institute of High Energy Physics, Beijing, China*
[d] *Université Libre de Bruxelles, Brussels, Belgium*
[e] *Tsinghua University, Beijing, China*
[f] *Guangxi University, Nanning, China*
[g] *School of Physics and Astronomy, Shanghai Jiao Tong University, Shanghai, China*
[h] *Tsung-Dao Lee Institute, Shanghai Jiao Tong University, Shanghai, China*
[i] *University of Chinese Academy of Sciences, Beijing, China*
[j] *Nanjing University of Aeronautics and Astronautics, Nanjing, China*
[k] *INFN Sezione di Catania, Catania, Italy*
[l] *Università di Catania, Dipartimento di Fisica e Astronomia, Catania, Italy*
[m] *INFN Sezione di Ferrara, Ferrara, Italy*
[n] *Università degli Studi di Ferrara, Dipartimento di Fisica e Scienze della Terra, Italy*
[o] *INFN Sezione di Milano e Università di Milano, Dipartimento di Fisica, Milano, Italy*

---

* Corresponding author at: Università di Padova, Dipartimento di Fisica e Astronomia, Padova, Italy.
 E-mail address: vonsturm@pd.infn.it (K. von Sturm).
 1 Now at INFN Laboratori Nazionali del Sud, Italy.

p *INFN Sezione di Milano Bicocca, e Università di Milano Bicocca, Dipartimento di Fisica, Milano, Italy*
q *INFN Sezione di Roma Tre e Università di Roma Tre, Dipartimento di Matematica e Fisica, Roma, Italy*
r *INFN, Sezione di Milano Bicocca e Politecnico di Milano, Dipartimento di Energetica, Milano, Italy*
s *INFN Sezione di Perugia e Università di Perugia, Dipartimento di Chimica, Biologia e Biotecnologie, Perugia, Italy*
t *Laboratori Nazionali dell'INFN di Frascati, Italy*

ARTICLE INFO

Keywords:
Electronics
Photomultiplier
Large scale neutrino experiment

ABSTRACT

The Jiangmen Underground Neutrino Observatory (JUNO) is a large neutrino detector currently under construction in China. JUNO aims to determine the neutrino mass ordering and to perform leading measurements detecting terrestrial and astrophysical neutrinos over a wide energy range, spanning from 200 keV to several GeV. Given the ambitious physics goals of JUNO, its readout electronics has to meet specific requirements, which motivated the thorough characterization described in this manuscript. The time synchronization among the electronics modules was found to exceed by few ns the theoretical expectation, as a consequence of the non-optimal data taking conditions. However, the system showed an excellent stability over long data taking periods, ensuring that any time offset could be calibrated out at the beginning of the data taking.

The maximal deviation from a linear charge response was found to be 1.1% for the high gain ADC and 0.8% for the low gain ADC. In a JUNO-like environment, i.e 40 m underwater, the recorded FPGA temperature complied with the reliability standards of JUNO.

1. Introduction

The Jiangmen Underground Neutrino Observatory (JUNO) [1] is a next-generation neutrino experiment under construction in South China, whose aim is to tackle unresolved issues in neutrino physics and astrophysics. The experiment has been proposed with the main goal of determining the neutrino mass ordering (NMO) at $3\,\sigma$ significance within six years of operation, and providing a measurement of the neutrino oscillation parameters with sub-percent precision [2].

The JUNO central detector (CD) contains 20 kton of liquid scintillator (LS), it is hosted in an underground laboratory (650 m overburden), and it aims to detect primarily electron antineutrinos produced by the 52.5 km-distant Yangjiang and Taishan Nuclear Power Plants. Particle interactions in the LS generate scintillation and Cherenkov photons, which are then converted into photo-electrons (PEs) by 17 612 20-inch Photomultiplier Tubes (PMTs) (*Large-PMTs*), and 25 600 3-inch PMTs (*Small-PMTs*). In addition, 2400 Large-PMTs are installed in the instrumented Water Pool detector, working as water Cherenkov muon veto system, in which the CD is immersed. A total of 15,000 20-inch MCP-PMTs were produced by Northern Night Vision Technology Co. (NNVT), and 5000 dynode PMTs by Hamamatsu Photonics K. K.(HPK), all of which were tested by the JUNO collaboration [3].

The initial design of the Large-PMTs electronics [4] and the following R&D program [5] were driven by the two most important JUNO physics requirement, namely to keep the detector energy resolution below 3% at 1 MeV, and the uncertainty on the energy scale below 1% [6]. For the JUNO electronics it meant to develop a readout system able to measure the PMT output charge with 10% precision at 1 photoelectron (PE), and to achieve an excellent linearity over a dynamic range spanning from 1 PE to several hundreds PEs.

The capability to reconstruct the event vertex with a precision of few tens of centimeters is another important requirement for JUNO, because it allows (1) to tag signal events through spatial coincidences, (2) to accurately define a fiducial region within the detector volume, and (3) to precisely map the spatial response of the detector. On the electronics side, this requirement brings the need to precisely reconstruct the arrival time of the scintillation photons onto the PMTs.

The electronics modules will be placed in sealed boxes at a maximum water depth of 43 m, making it impossible to repair or access them after installation. As JUNO is expected to collect data for over a decade, the reliability of its readout electronics was one of the main concerns during the design phase, which translated into a careful selection of the electronics components in order to reach a maximum failure rate of 0.5% over 6 years of operation.

Several tests were performed in order to verify the Large-PMTs electronics specifications [7], which are required to fulfill the JUNO physics goals, as detailed in the following sections.

2. JUNO large-PMT electronics

A schematic of the JUNO Large-PMT electronics is given in Fig. 1; the design is an optimization of previous developments [5]. The full electronics chain is composed of two parts: the *front-end* (FE), or *wet* electronics, located very close to the PMT output, inside the JUNO Water Pool; and the *dry* electronics, installed in the electronics room of the JUNO underground laboratories, and consisting of the *back-end* (BE), or trigger, electronics and the data acquisition (DAQ) system. The FE electronics will be installed underwater on the JUNO Steel Truss structure, inside a stainless steel, water-tight box, the so-called Under Water Box (UWbox). The JUNO detector will be instrumented with 6681 UWboxes, 5878 for the CD and 803 for the Water Pool, as part of the JUNO Veto system.

Three PMT output signals are fed to one UWbox which contains:

- three High Voltage Units (HVU): programmable modules which provide the bias voltage to the PMT voltage divider. Each HVU independently powers one Large-PMT. The HVUs are mounted on a custom Printed Circuit Board (PCB), the splitter board, that provides mechanical stability to the modules, and decouples the PMT signal current from the high voltage.
- a Global Control Unit (GCU): a motherboard incorporating the Front-End and Readout electronics components. The three PMT signals reaching the GCU are processed through independent readout chains.

The PMT analog signal reaching the GCU is processed by a custom Front-End Chip (FEC), which splits the input signal and amplifies it with two different gains, referred to as low-gain and high-gain (see Fig. 1). The two signals are further converted to a digital waveform by a 14 bit, 1 GS/s, custom Flash Analog-to-Digital Converter (FADC).

The usage of two FADCs per readout channel is driven by the stringent requirements on the charge resolution to be achieved over a wide dynamic range, namely a 0.1 PE resolution between 1 PE and 100 PEs (high-gain stream), and 1 PE resolution between 100 PEs and 1000 PEs [1].

A Xilinx Kintex-7 FPGA (XC7K325T) is the core of the GCU and allows to process the digital signal (local trigger generation, charge reconstruction and timestamp tagging) and temporarily store it in a local memory buffer before sending it to the DAQ. Besides the local memory available in the readout-board FPGA, a 2 GB DDR3 memory is available and used to provide a larger memory buffer in the exceptional case of a sudden increase of the input rate, which would otherwise overrun the current data transfer bandwidth between the FE electronics and the DAQ.
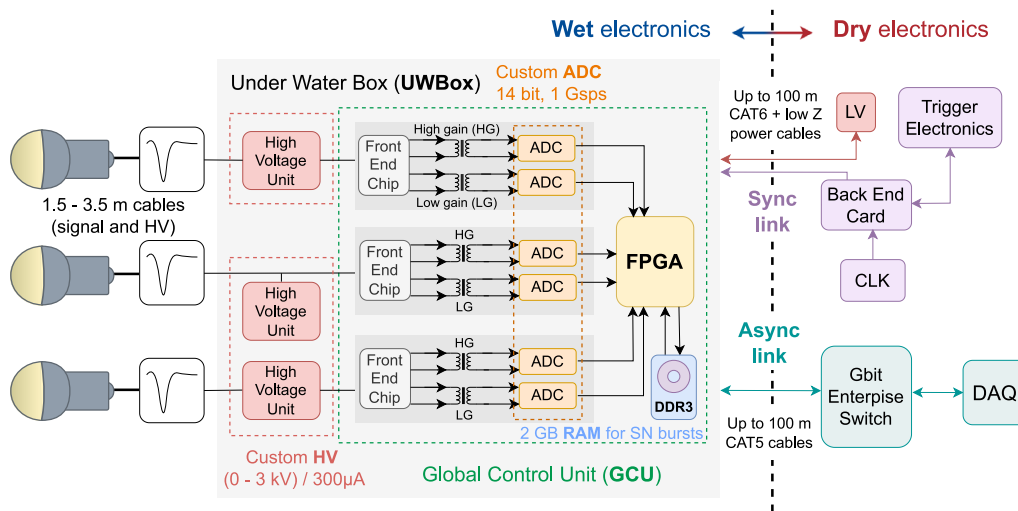
Fig. 1. JUNO large PMT electronics Read-Out electronics scheme. A description of the different parts is given in the text.

An additional Spartan-6 FPGA (XC6SLX16) is available on the same motherboard. It implements a 2-port Ethernet hub and a RGMII interface between the PHY network chip and the Spartan-6, which also interconnects the Spartan-6 and the Kintex-7. The Spartan-6 FPGA provides an important failsafe reconfiguration feature of the Kintex-7 by means of a virtual JTAG connection over the IPbus, removing the need of a dedicated JTAG connector and cable.

The BE electronics is composed of the following active elements:

- the Back End Card (BEC) with the Trigger and Time Interface Mezzanine (TTIM)
- the Reorganize and Multiplex Units (RMU) and the Central Trigger Unit (CTU), which are part of the Trigger Electronics.

The PMTs are connected to the UWbox electronics with a $50\,\Omega$, coaxial cable, with a fixed length of $2\,m$ for the CD PMTs and $4\,m$ for the VETO PMTs [3]. The electronics inside the UWbox has two independent connections to the BE electronics: a so-called *synchronous link* (S-link), which provides the clock and synchronization to the boards and handles the trigger primitives, and an *asynchronous link* (A-link) which is fully dedicated to the DAQ and slow-control, or Detector Control System (DCS). These connections are realized using commercially available CAT-5 and CAT-6 Ethernet cables for the A-link and S-link, respectively; the length of the cables ranges between $30\,m$ and $100\,m$. An additional, low-resistance, power cable will be used to bring LV power to the electronics inside the UWbox.

The Large-PMT electronics runs by default in *global trigger* mode, where the information from the single *fired* PMTs is collected and processed in the Central Trigger Unit (CTU). The latter validates the trigger based on a simple PMT multiplicity condition or a more refined topological distribution of the fired PMTs in JUNO. Upon a trigger request, validated waveforms are sent to the DAQ event builder through the A-link. The IPBus Core protocol is used for data transfer, slow control monitoring, and electronics configurations [8].

An alternative running mode is possible, where all readout boards send their locally triggered waveforms to the DAQ, independently of each other. With this approach, all the digitized waveforms, including those generated by the PMT dark noise, will be sent to the DAQ.

3. Experimental setup overview

To validate the full electronics performance, a medium size setup with 48 independent channels was built and operated at the Legnaro National Laboratories (LNL) of the Italian National Institute of Nuclear Physics (INFN).

3.1. Small-scale test setup

The apparatus is composed of a cylindrical acrylic vessel, made of transparent Plexiglass, with inner dimensions of 25 cm diameter and 35 cm height, filled with about 17 L of liquid scintillator (LS). The liquid scintillator is composed of a solvent, linear alkylbenzene (LAB), doped with Poly-Phenylene Oxide (PPO) and p-bis-(o-MethylStyryl)-Benzene (bisMSB), used as wavelength shifter to match the PMT response; the LS mixture has been optimized using one detector of the Daya Bay experiment [9]. The LS vessel is inserted in a coaxial larger cylindrical structure that supports 48 2-inch photomultipliers arranged in three rings, with 16 PMTs each. The inner vessel is surrounded by a black plastic structure that supports the PMTs and shields the liquid scintillator vessel from the external light. A drawing of the test system mechanical design and its realization can be found in Figs. 2 and 3, respectively.

The PMTs are Philips XP2020 with custom base, operated with the photocathode at negative high voltage and the anode at ground.[2] The PMTs feature a good linearity, a very low background noise (the typical dark noise is up to 900 Hz), and extremely good time characteristics [10].

The setup is equipped with ancillary systems (e.g., plastic scintillators to trigger on cosmic muons) that can be exploited to induce signal pulses on the PMTs; specifically, in this paper, we discuss some results obtained using a laser light source introduced inside the liquid scintillator vessel via an optical fiber and a diffuser. It allows to generate narrow pulses and is well suited to investigate the timing characteristics of the electronics.

3.2. Electronics chain

Electronic signals proportional to the charge collected by the PMTs are sent through several steps of the electronics chain, before being stored on disk. The 48 PMTs are connected, in groups of 3, to 16 GCUs; only 13 GCUs were available for the measurements described in the following sections (i.e., 39 acquisition channels). The electronics chain, whose schematic description is reported in Fig. 4, works according to the following steps:

- all three channels acquire their signals concurrently;

---

[2] This is the opposite of what is done in JUNO where the photocathode is at ground, while the anode is operated at positive high voltage.
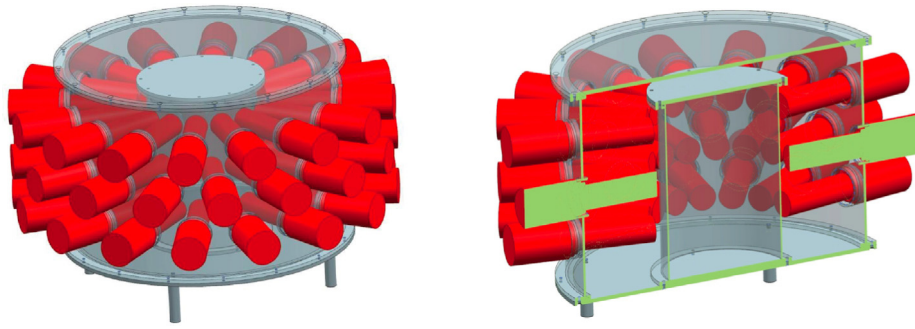
Fig. 2. Mechanical design of the test facility; the internal cylindrical vessel (gray) is surrounded by the 48 PMTs (red); the PMTs are inside the plastic structure (gray), while their bases are outside.
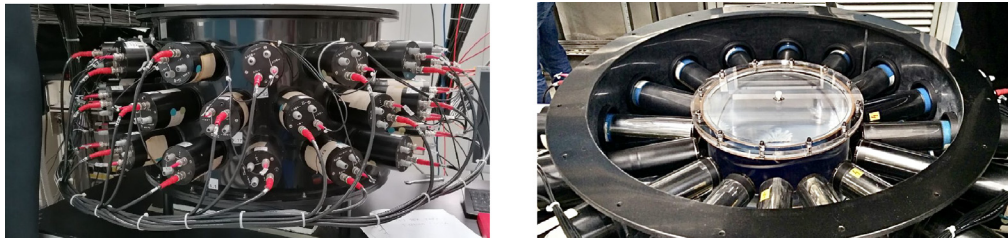

Fig. 3. Picture of the test facility: the black plastic structure and the PMTs base (on the left), the liquid scintillator vessel and the PMTs (on the right) are visible.
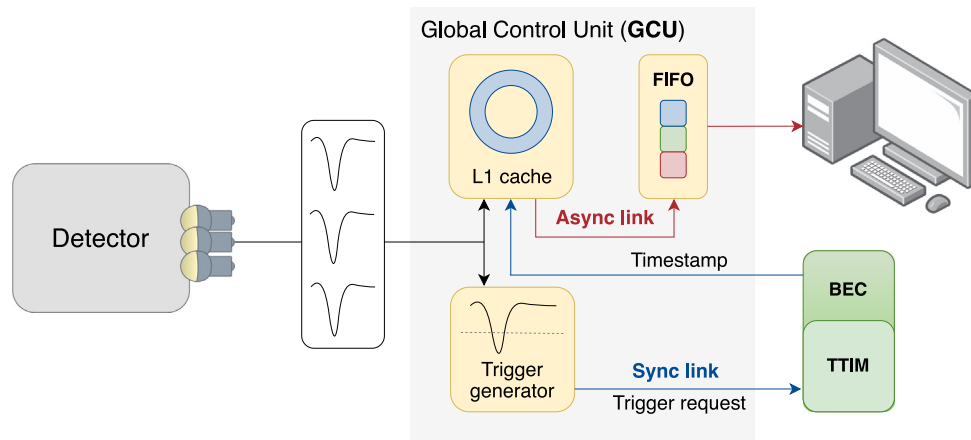

Fig. 4. Electronics chain.

- inside the GCU, each PMT analog signal is processed by a Front-End Chip, which splits the signal into two streams with different gain: a low-gain stream with a dynamic range going from 100 PEs to 1000 PEs, and a high-gain stream with a reduced range from 1 PE to 100 PEs. The signals are then fed to the FADC;
- inside the FPGA the digitized signal is split: one of the two signal copies is registered with its GCU timestamp on the L1 cache, while the other is analyzed with a specific threshold trigger algorithm;
- if the signal exceeds a fixed threshold, the GCU sends a trigger request to one BEC which collects the S-links from 48 GCUs. The TTIM then takes a *global trigger* decision, based on the chosen trigger logic, and sends a global trigger validation signal to all connected GCUs; for this step, GCUs and BEC must be properly synchronized in time [11]. Namely, the global trigger logic can be based either on a logic OR of all 3 channels of a single GCU, or on the multiplicity of the acquired event, i.e., a logic AND between two or more channels, either of the same GCU or of different ones. Besides this trigger validation procedure, the system implements

an additional external trigger that can be used, for instance, to trigger on different types of events;
- after the trigger validation by the BEC, the firmware retrieves the signals with the selected timestamp from the L1 cache and moves them to a First-In-First-Out (FIFO) unit. The content of the FIFO is then transferred to the server through a Gigabit Ethernet switch, where the DAQ program stores the raw data according to a fixed structure. Data transfer is implemented via the IPBus Core protocol [12]. An in-depth investigation of the implementation and performance of the IPBus in the JUNO data acquisition streams can be found in [8].

The BE presents some differences with respect to the final JUNO back-end chain. Since the detector has been set up during the electronics development phase, different components were not yet available or fully functional; therefore, the BE initially included only the BEC and TTIM. For this reason, a special TTIM FPGA configuration was developed, which included all the basic trigger decision functionalities and the IPBus connectivity. Nevertheless, this temporary
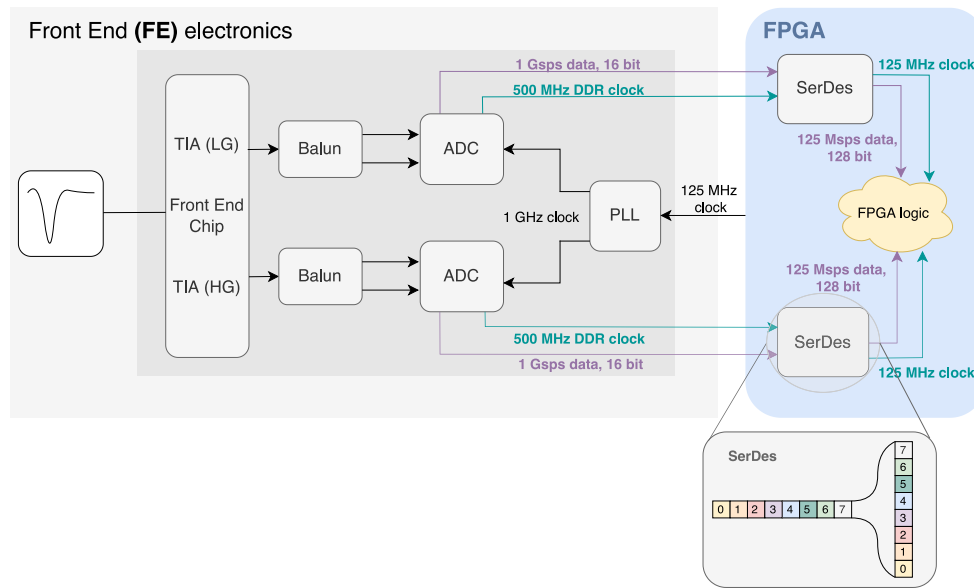
Fig. 5. Block diagram of the FE. The FE electronics provides the FPGA with a 14 bit parallel bus synchronous to its 500 MHz DDR sampling clock. The inset graph represents the SerDes tile behavior in the Input/Output Blocks (IOB): it groups together 8 ADC words, synchronizing them to a system clock of 125 MHz.

dedicated firmware includes the back-end module for the IEEE 1588 synchronization protocol [11].

4. Timing synchronization

All the GCUs in JUNO must share a common global time in order to correctly timestamp the PMT waveforms resulting from a given energy deposition in the detector. To this end, a common 125 MHz clock is distributed to all the GCUs. The clock network is based on the *White Rabbit* (WR) standard, which exploits the IEEE 1588-2008 Precision Time Protocol (PTP) to synchronize the local (front-end) and global (back-end) clocks with a precision of ±1 clock period [11]. This means that two GCUs are time aligned within a time window of ±8 ns.

As described in Section 3.2, the FADC digitizes the PMT output waveform and sends it to the FPGA for further processing. A block diagram of the FE electronics is shown in Fig. 5. A stream of 14-bit data, sampled at 1 Gsample/s, is transferred from the ADC to the FPGA, with the data synchronized to a 500 MHz Double Data Rate (DDR) sampling clock. The latter is generated by a Phase-Locked-Loop (PLL) mounted on the FADC, which receives the system clock from the GCU and provides a low jitter 1 GHz clock to the ADC. As a result of the system clock running at 125 MHz, each PLL has a phase uncertainty of 8 ns.

The FPGA logic is not able to sustain a stream of 1 Gsample/s 14-bit ADC data, therefore a Serializer/Deserializer (SerDes) is used to handle the input stream. The SerDes parallelizes the incoming data 8 to 1, so that a 1 Gsample/s 16-bit data stream (14 bit ADC + 2 bit padding) is parallelized into a 125 Msample/s 128-bit data stream. The SerDes behavior is depicted in the inset of Fig. 5, and it results in an additional 8 ns phase uncertainty for each channel.

As a result of the GCU features described above, two simultaneous PMT pulses will result into two digitized pulses not aligned in time. The time difference caused by the inherent phase uncertainty of the PLL and by the serialization of the ADC output when entering the FPGA (SerDes) is expected to be up to 16 ns.

Additionally, if the two pulses are recorded by channels hosted on different GCUs, an extra 16 ns offset could be present as a result of the intrinsic precision of the IEEE 1588-2008 intra-GCU synchronization protocol.

The resulting maximum absolute deviation between to simultaneous input pulses is expected to be:

- 16 ns for channels of the same GCU.
- 32 ns for channels residing on different GCUs.

4.1. Synchronization test

For a proper operation of the system, synchronization among the GCUs has to be stable over time: since it is possible to perform the timing realignment at the start of each run, it is sufficient to assure stability within one single run. To evaluate the timing synchronization and mismatch between GCU channels, the 48 PMT small-scale setup was used: this is equipped with extremely fast PMTs, suitable for this kind of measurement (they are characterized by a time jitter of ∼250 ps [10]). A laser source was employed for the test, the Hamamatsu PLP-10 ultrashort pulsed light source was used: it consists of an M10306 laser diode head and a C10196 controller which provides fast pulses with a FWHM of about 52 ps at a wavelength of 403 nm [13], value that is close to the maximum sensitivity of the PMTs.

The laser timing was first checked by injecting laser pulses into the LS and directly verifying the alignment of the rising edges of signals detected by the single PMTs. The time offsets with reference to a fixed channel are measured by means of an oscilloscope and range from a maximum of (2.4 ± 0.5) ns to a minimum of (-1.1 ± 0.2) ns, which can be considered negligible with respect to the expected timing mismatch. Moreover, the PMT hit time is not affected by the laser injection position: indeed no correlation was found with the position of the PMTs inside the three rings.

The test setup for the GCU acquisition is shown in Figs. 4 and 6, where the electronics chain and the pulse injection synchronization signal are detailed, respectively. The BEC is set in external trigger mode, connected to the external trigger output of the laser pulse generator; the laser frequency is set to 2 Hz for the test. Each time the light is emitted, the associated timestamp is received from the BEC via the synchronous link as a global trigger validation, marking the start of the event.

As a result of the effects described at the beginning of Section 4, waveforms acquired by different channels are not perfectly synchronized, but present an offset. With the purpose of evaluating the latter, the time differences between the trigger time[3] of the ith channel and that of a reference channel are evaluated.

---

[3] Timestamp in which the signal reaches an amplitude of 5 σ above its baseline; σ is the standard deviation of the baseline distribution calculated over a fixed number of samples (as detailed in Section 5).
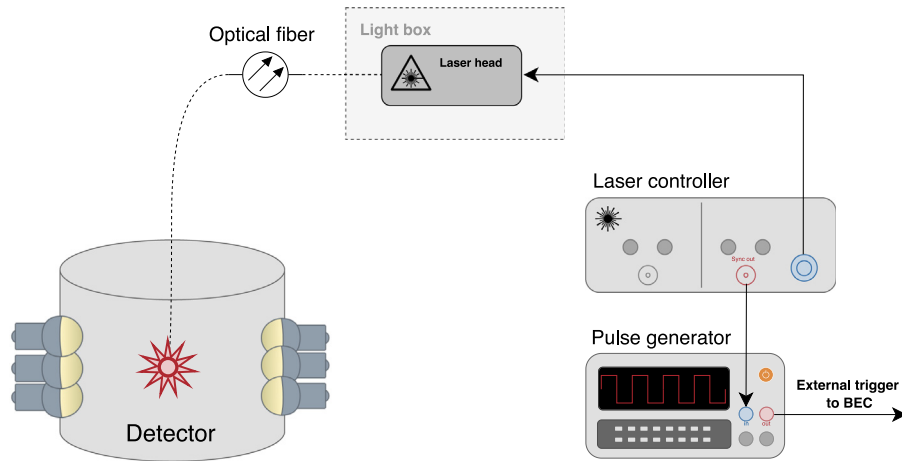
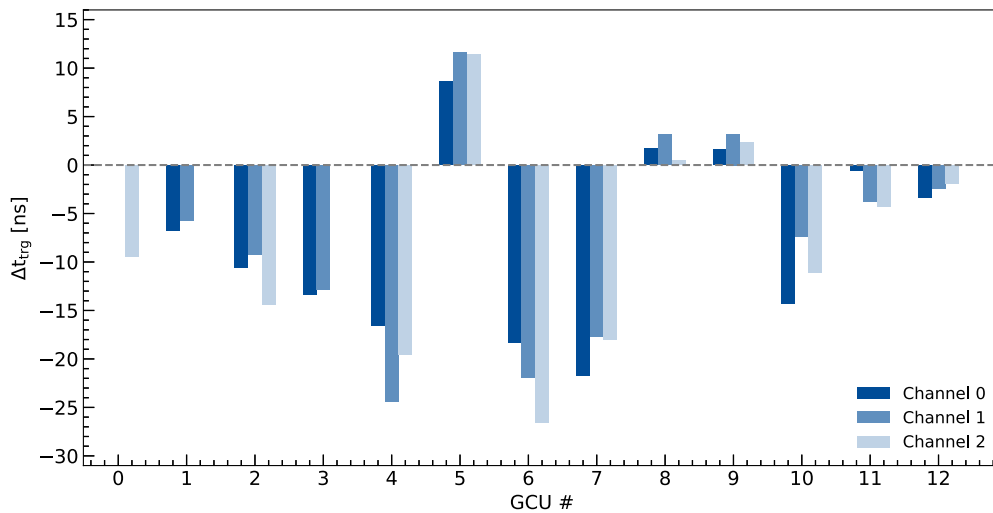**Fig. 6.** Test setup with the laser source for the synchronization measurements.

Fig. 7. Average time differences Δt_{trg} for different channels with respect to a fixed one (ch1 of GCU0).
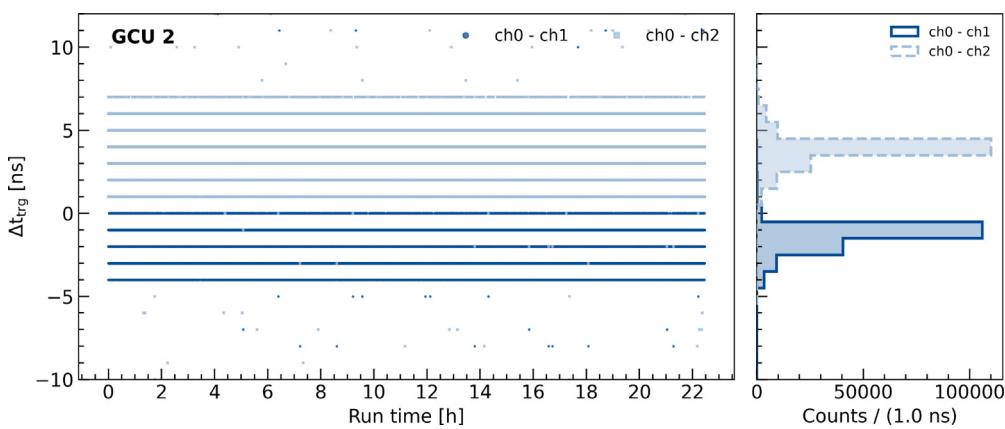

Fig. 8. Average time differences Δt_{trg} for two channels of the same GCU, during roughly 22 h. In this case GCU2 is under study and the differences are calculated for channels 1 and 2 with respect to channel 0. The Δt_{trg} distributions (on the right panel) are peaked around -1.5 ns and 4 ns for channels 1 and 2, respectively. Some outliers, not visible in the plot, are found at more than $3\,\sigma$ from the mean value represented only $\sim 2\%$ of the sample. The same behavior is observed for the other channels.

The analysis was conducted evaluating the time differences Δt_{trg} for all 37 channels and choosing channel 1 of GCU0 as reference. All average Δt_{trg} for the different channels are shown in Fig. 7. Firstly, one can infer that channels residing on the same GCU are synchronized within a time interval ≤ 10 ns, well inside the expected 16 ns. This

aspect is further illustrated in Fig. 8, where Δt_{trg} is evaluated for channels 1 and 2 of GCU2 (used as an example) throughout a one day-long acquisition, and choosing channel 0 as reference.

However, looking at Fig. 7, results show that the majority of the signals deviate in time from the reference trigger time by values that
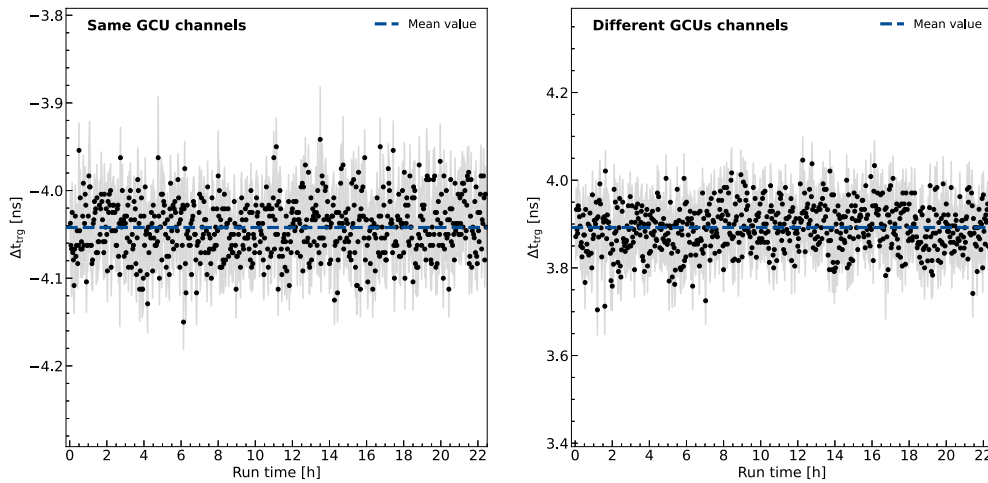
Fig. 9. Trigger time difference Δt_{trg} stability during a one day-long acquisition: left-hand side results for two channels of the same GCU, right-hand side for two channels of different GCUs. Each point represents the mean value of a 2 min sample; error bars indicate the standard deviation of the corresponding distribution.
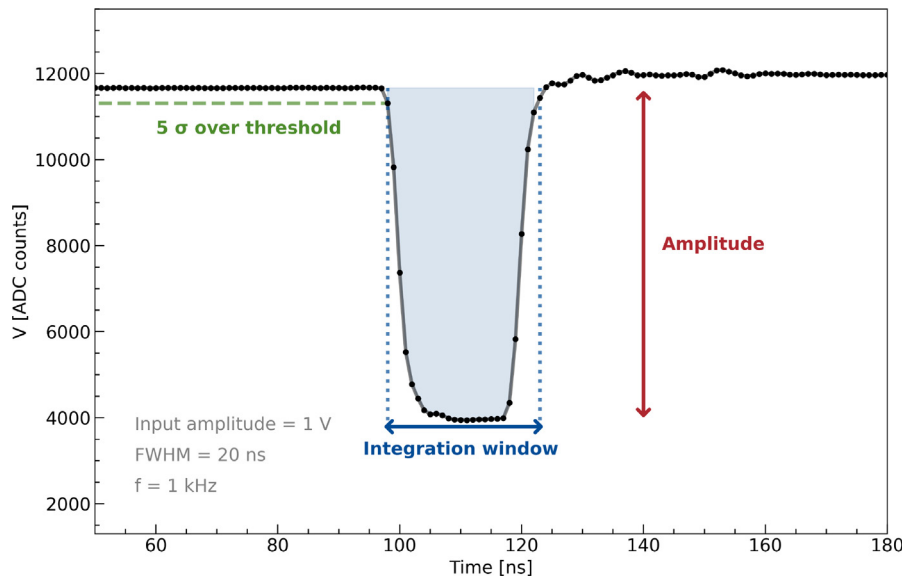

Fig. 10. Example of typical reconstructed waveform obtained using the pulse generator. The integration window is represented by the shaded area. The pulse width at Full Width Half Maximum (FWHM) and the signal amplitude are indicated as well. The mean of the pre-trigger sampled points, above the 5 σ trigger threshold displayed in dashed green, provide an estimate of the baseline (B in Eq. (1)).

range from ~-26.5 ns to ~ 11.5 ns, summing up[4] to ~ 38 ns. The maximum deviation expected by the response of the readout system is exceeded by roughly 6 ns. One possible explanation for this extra deviation is the asymmetry of the Cat-5E twisted pairs that provide the physical communication link between the FE and the BE, because the time synchronization performance of the IEEE 1588-2008 PTP protocol is known to be prone to this weakness [14,15]. However, we did not investigate thoroughly the actual source of this extra time difference, because the most important feature of this offset is to be constant over time (see below), meaning that it can be corrected via time calibration at the beginning of the data taking.

The stability of the synchronization between different GCUs was studied by evaluating the trigger time differences over several day-long runs. An example is reported in Fig. 9: the channels remain synchronized throughout the whole acquisition period, which means that once the alignment is performed, the difference in the trigger time

remains stable within the predicted uncertainty. This result makes us confident that the channel-to-channel time deviations shown in Fig. 8 will not affect JUNO physics performance.

5. Charge linearity

The determination of the NMO requires the energy resolution of JUNO to be better than 3% at 1 MeV [1], and the energy scale to be known better than 1%. To measure the intrinsic non-linear behavior of the scintillation and Cherenkov light emitting mechanisms a comprehensive calibration program [16] is foreseen. The PMTs and their readout electronics are also known to suffer from a non-linear response in the case of large detected charge. To assess the linearity of the readout electronics we performed the following test.

We used an external pulse generator to feed a GCU with square wave signals with rise and fall times of 2 ns, a width of 20 ns, frequency of 1 kHz and amplitudes spanning from roughly 500 mV to 3 V. The input charge in pC was computed considering the above-mentioned parameters and an output impedance of 50 Ω.

An example of the reconstructed waveform is shown in Fig. 10.

---

[4] In this way it is possible to assess the configuration with the largest possible spread one can find by randomly choosing 2 GCUs for the calculation of Δt_{trg}.
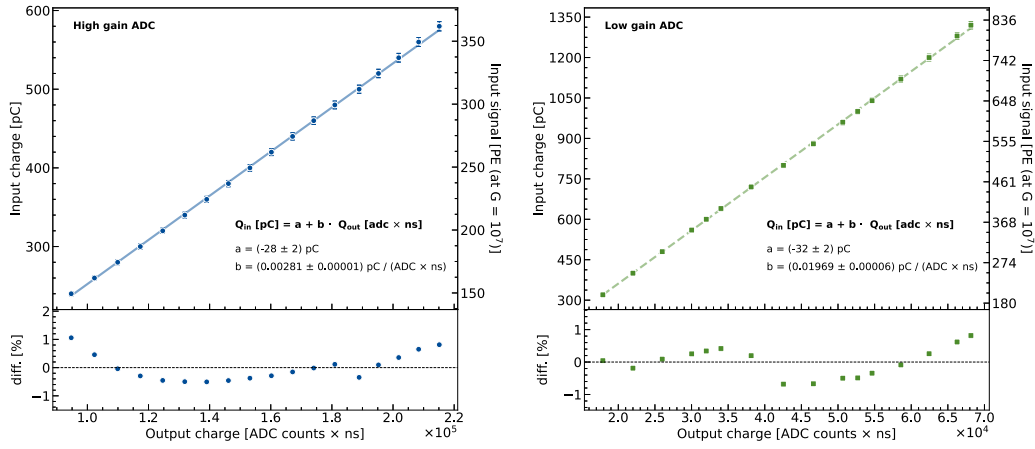
Fig. 11. Linearity of one of the channels for the high gain ADC (on the left), and the low gain ADC (on the right). The top panel shows the calibration curve for the two ADCs with the best fit values; in the bottom panel the relative error is reported: diff [%] = $\frac{y_{data}-y_{fit}}{y_{fit}}$. The uncertainties on the input charge are obtained through propagation, considering the specifications of the employed external pulser.
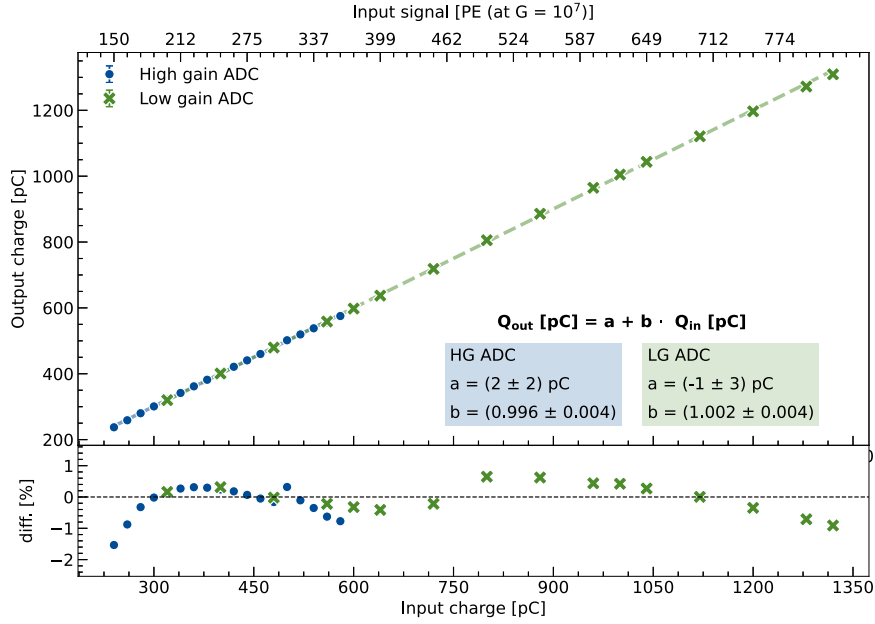

Fig. 12. Linearity plot with calibrated data. As reference, the input charge x-scale is also given in PE units, assuming a PMT gain of 10^7.

The output charge (Q_{out}) was reconstructed by calculating the integral of the signal waveform within a fixed time interval, corresponding to a certain number of samples N_s, which can be modified during acquisition via the IPbus protocol:

$$Q_{out} \; [ADC \times ns] = \sum_{i=1}^{N_s} |N_i - B| \cdot \Delta t_i \qquad (1)$$

where N_i is the content of the ith sample in ADC counts, B is the baseline mean value evaluated on a fixed number of samples in the pre-trigger region (e.g., first 50 samples) and Δt_i is equal to the sampling time (i.e., 1 ns). Both baseline and signal time windows were fixed for all events in an acquisition run. In this context, the integration window extremes were determined as the time instants when the signal falls below a threshold of 5 σ from the baseline. Therefore, for each event, the output charge mean value and its associated uncertainty (standard deviation divided by the square root of the number of pulses) were retrieved.

In Fig. 11 the calibration curve for a single channel and both FADCs is shown: the plot shows good linearity and the maximal deviation from a linear fit is ~1.1% for the high gain ADC and ~0.8% for the low gain

ADC. The systematic trend of the residuals in the bottom panel are most likely due to ADC Differential Non-Linearity.

The calibration parameters retrieved from the linear regression are then used to convert the output charge in pC. In Fig. 12, the linear response of the electronics is assessed by comparing the input and output charge. As reference, the input charge scale is also given in PE units, assuming the nominal PMT gain of the 20-inch PMTs in JUNO [3], i.e., $G_{PMT} = 10^7$. In this test, and mainly for the high gain stream ADC, it was not possible to extend the dynamic range to lower PE levels, due to instrumental limitations.[5]

The superposition (Fig. 12) of the high and low gain ADCs curves highlights the goodness of the calibration parameters estimation. The maximal deviation from a linear fit is ≃2%.

Furthermore, within the mass testing of the readout electronics, the linearity response was evaluated for about 6900 GCUs, by injecting PMT-like signals with an internal test pulse circuit: a typical distribution for the gain of both streams ADCs can be found in [17].

---

[5] The poor resolution at low voltage input signal (≤100–150 mV) would have introduced an irreducible instrumental non-linearity.
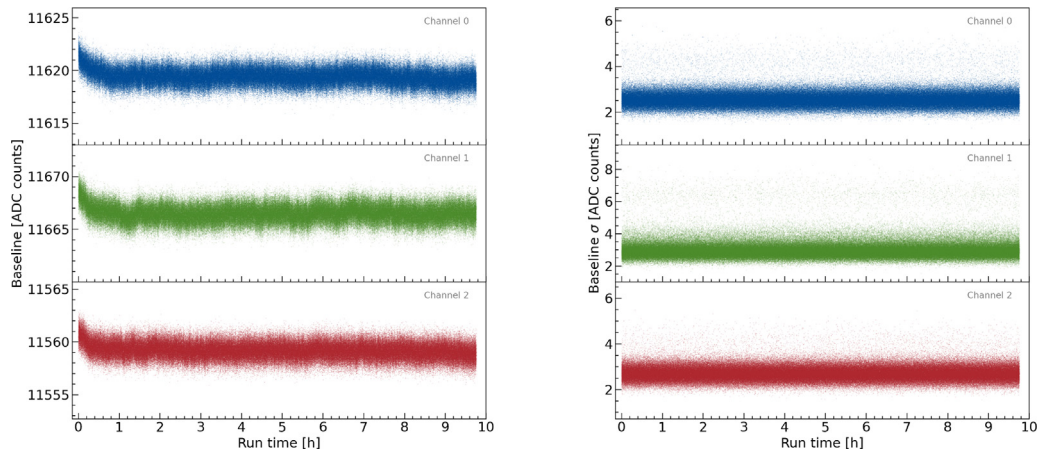
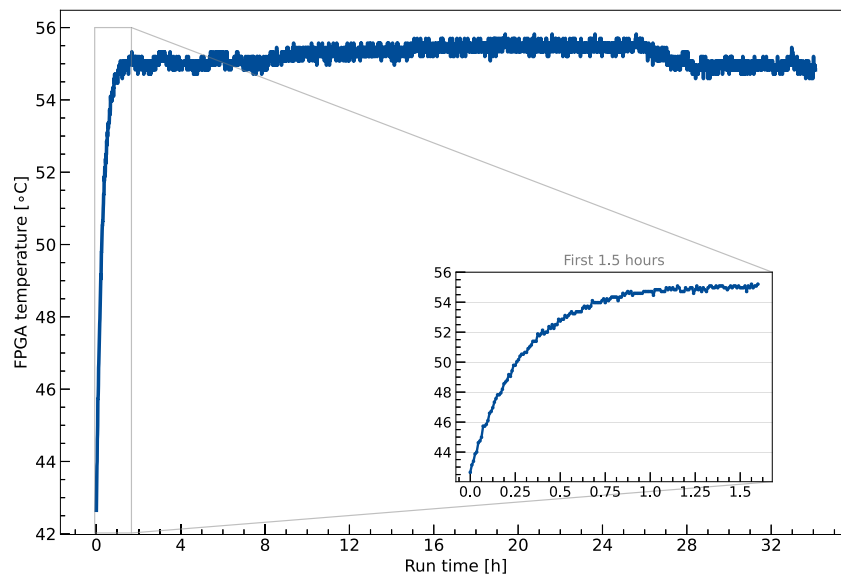**Fig. 13.** First 10 h trend of baseline value (left) and baseline standard deviation (right).

Fig. 14. FPGA temperature monitoring over the ~32 h acquisition. The inset plot shows the increasing trend in the first 1.5 h of the test. The temperature stabilizes after roughly two hours.

6. UWBox deep-water test

A further electronics and mechanical verification was performed thanks to a collaboration with the *Y-40 The Deep Joy* pool in Montegrotto Terme [18], one of the deepest thermal water pools in the world, with its 42.15 m depth. The box stayed underwater at the bottom of the pool for roughly 30 h with no PMT connected to it. During this time, the FPGA and HVU temperatures were monitored, as well as the baseline average value and standard deviation. Since no BEC was used, a modified GCU-standalone version of the firmware that did not require the synchronous link was developed. The board was set in auto-trigger mode, where calibration pulses, a feature foreseen in the FEC, were triggered remotely via IPBus.

In Fig. 13, results are reported for all three active channels for the baseline mean (left) and standard deviation (right). Moreover, the temperature read from an internal sensor of the FPGA was recorded: as shown in Fig. 14, after a fast initial increase, it stabilizes at about 55 °C, with a water temperature of roughly 33 °C, resulting in a difference of about 22 °C. Since the water temperature in JUNO is foreseen to be around (21 ± 1.4) °C [6], the FPGA temperature should be below 45 °C; since the FPGA temperature is more than 15° higher than that of the board, it falls within the reliability requirements. Indeed, the

UWBox cooling should prevent the environment temperature inside the box from exceeding 30 °C [15] when in water.

The above-mentioned plots show a correlation between baseline mean value and temperature: as the latter rises, the former decreases, until both of them reach a stable value that remains constant during the acquisition. Nevertheless, the water temperature in JUNO is kept constant and therefore no changes in the GCU's temperature are expected. The baseline standard deviation value remained unchanged throughout the entire test.

7. Conclusions

Several tests were performed to assess the performance of the JUNO Large-PMTs electronics. Synchronization among the GCUs, a key requirement to fulfill the ambitious goals of JUNO, was investigated and monitored over time. The results of the measurements reveal a good agreement with the expected time synchronization performance: the maximum timing mismatch turned out to be ~38 ns, which exceeds by roughly 6 ns the theoretical prediction. The most important feature of this time offset turned out to be its stability over time, meaning that it will possible to calibrate it out at the beginning of the data taking.

The linearity response of electronics was also evaluated: the maximal deviation from a linear fit is ~1.1% for the high gain ADC, in the

range (150–350) PEs and ∼0.8% for the low gain ADC, in the range (200–800) PEs.

Additionally, the UWBox was tested ∼40 m underwater, in order to verify its behavior in a JUNO-like environment. The acquired data is consistent with the system's proper operation, and the FPGA recorded temperature complies with the reliability standards.

Declaration of competing interest

The authors declare that they have no known competing financial interests or personal relationships that could have appeared to influence the work reported in this paper.

Data availability

The authors are unable or have chosen not to specify which data has been used.

Acknowledgments

References

[1] Fengpeng An, et al., JUNO Collaboration, Neutrino Physics with JUNO, J. Phys. G 43 (3) (2016) 030401, http://dx.doi.org/10.1088/0954-3899/43/3/030401, arXiv:1507.05613.

[2] Angel others Abusleme, Sub-percent precision measurement of neutrino oscillation parameters with JUNO, Chin. Phys. C 46 (12) (2022) 123001.

[3] Angel Abusleme, et al., Mass testing and characterization of 20-inch PMTs for JUNO, Eur. Phys. J. C 82 (12) (2022) 1168.

[4] Z. Djurcic, et al., JUNO Conceptual Design Report, 2015, arXiv:1508.07166.

[5] M. Bellato, et al., Embedded readout electronics R&D; for the large PMTs in the JUNO experiment, Nucl. Instrum. Methods A 985 (2021) 164600, http://dx.doi.org/10.1016/j.nima.2020.164600, arXiv:2003.08339.

[6] A. Abusleme, et al., JUNO Collaboration, JUNO physics and detector, Prog. Part. Nucl. Phys. 123 (2022) 103927, http://dx.doi.org/10.1016/j.ppnp.2021.103927, arXiv:2104.02565.

[7] Vanessa Cerrone, JUNO Collaboration, Characterization of JUNO Large-PMT electronics in a complete small scale test setup, PoS ICHEP2022 (2022) 1112, http://dx.doi.org/10.22323/1.414.1112.

[8] Riccardo Triozzi, et al., Implementation and performances of the ipbus protocol for the juno large-PMT readout electronics, 2023, arXiv preprint arXiv:2302.10133.

[9] A. Abusleme, et al., Optimization of the JUNO liquid scintillator composition using a daya bay antineutrino detector, Nucl. Instrum. Methods A 988 (2021) 164823.

[10] Philips, XP2020 photomultiplier tube, 1986, URL https://wwwusers.ts.infn.it/~rui/univ/Acquisizione_Dati/Manuals/Philips%20XP2020.pdf.

[11] D. Pedretti, et al., Nanoseconds Timing System Based on IEEE 1588 FPGA Implementation, IEEE Trans. Nucl. Sci. 66 (7) (2019) 1151–1158, http://dx.doi.org/10.1109/TNS.2019.2906045.

[12] C. Ghabrous Larrea, K. Harder, D. Newbold, D. Sankey, A. Rose, A. Thea, T. Williams, IPbus: a flexible Ethernet-based control system for xTCA hardware, JINST 10 (02) (2015) C02019, http://dx.doi.org/10.1088/1748-0221/10/02/C02019.

[13] Hamamatsu, PLP-10 laser diode head series, 2021, URL https://www.hamamatsu.com/resources/pdf/sys/SOCS0003E_PLP-10.pdf.

[14] IEEE standard for a precision clock synchronization protocol for networked measurement and control systems, IEEE Std 1588-2008 (Revision of IEEE Std 1588-2002) (2008) 1–269, http://dx.doi.org/10.1109/IEEESTD.2008.4579760.

[15] Filippo Marini, Development and Testing of the large PMTs Front-End Electronics for the JUNO Experiment (Ph.D. thesis), University of Padua, Italy, 2021, URL https://hdl.handle.net/11577/3443916.

[16] Angel Abusleme, et al., Calibration strategy of the JUNO experiment, J. High Energy Phys. 2021 (3) (2021) 1–33.

[17] Alberto Coppi, et al., Mass testing of the JUNO experiment 20-inch PMT readout electronics, Nucl. Instrum. Methods A (2023) 168255, http://dx.doi.org/10.1016/j.nima.2023.168255.

[18] Y-40 the deep joy, URL https://www.y-40.com/en/.